

Flow Around a Tethered Body: The Effect of Tether Length

Kris Ryan,

Fluids Laboratory for Aeronautical and Industrial Research (FLAIR)

Department of Mechanical and Aerospace Engineering, Monash University, Victoria, Australia

Kris.Ryan@eng.monash.edu.au

The tethered cylinder may be considered an extension of the more familiar (and widely studied) freely oscillating cylinder. In particular, assuming that the tether does not provide significant mechanical damping it directly extends the work of Khalak and Williamson (1999), Govardhan and Williamson (2000) and Govardhan and Williamson (2003). In particular, as with a lightly damped oscillating cylinder, the tethered cylinder system exhibits a critical mass ratio, below which large amplitude oscillations are observed (Ryan *et al.* 2007). This critical mass ratio is observed to vary as a function of tether length. As part of their work, Ryan *et al.* (2007) observed a peak in maximum oscillation amplitude (for the particular case of $m^* = 0.2$) at a tether length ratio of $L^* \approx 2.0$. However, no explanation for this local maximum was presented therein. This paper explores the reasons for this local peak, in addition to describing the structures in the wake of the cylinder as a function of tether length.

Figure 1 describes the geometry of the problem. A cylinder is attached to a mass-less, inflexible tether whose length may be described as the length ratio, $L^* = L/D$; Where L is the length of the tether, and D is the diameter of the cylinder. An additional controlling parameter is the cylinder mass ratio, m^* , defined as the ratio of the density of the cylinder to that of the working fluid. The equation of motion for the system may be written as

$$J\ddot{\phi} + (T)L^*D\dot{\phi} = F_{osc}L^*D, \quad (1)$$

where J is the moment of inertia of the tethered body system, T is the tension within the tether, F_{osc} describes the fluid force acting to oscillate the body and ϕ describes the angular oscillation of the system about the mean layover angle θ . Details of the system may be found in Ryan *et al.* (2007). In particular, the moment of inertia is defined exactly as

$$J = mD^2\left(L^{*2} + \frac{1}{8}\right), \quad (2)$$

with m representing the mass of the cylinder.

This system was simulated in two dimensions through the solution of the Navier-Stokes equations, written in primitive variable form, using a spectral element method. The cylinder motion

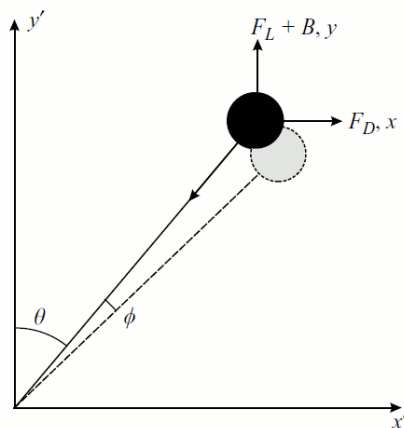


Figure 1. Tethered cylinder geometry and coordinate system.

is calculated in an inertial reference frame centred on the cylinder, negating any need for deforming or moving meshes. The equations of motion (equation 1) are coupled with the Navier-Stokes equations through an Adams-Bashforth/Adams-Moulton predictor-corrector technique, which updates the cylinder position several times for each time-step. Details of the solution technique are may be found in Ryan *et al.* (2007) and references cited therein.

To agree with the prior work of Ryan *et al.* (2007), we restrict our attention to $Re = 200$ (where the Reynolds number is based on the cylinder diameter). In addition, we consider only one mass ratio, $m^* = 0.2$ and a wide range of tether length ratios, $L^* = [0.1, 10]$. The tether length is measured from the centre of the cylinder, such that for $L^* = 0.5$, the cylinder is oscillating about a pivot point attached to its surface. The computational grid consists of 518 macro-elements; the inlet being 15 diameters upstream of the leading edge of the cylinder, and the outlet 23 diameters downstream of the trailing edge of the cylinder. Domain side-walls are 30 diameters apart. Seventh order polynomials were used as interpolating polynomials within each macro-element.

Typically, the controlling parameter considered for freely oscillating bodies is the reduced velocity $U^* = U/f_n D$, where f_n is the natural frequency of the system, and U is the inlet velocity. However, for most cases, the natural frequency cannot be determined *a priori* for the tethered body system, as it is dependent on the tension acting through the tether, and hence on the fluid forces acting on the system. Instead, we follow the work of Ryan *et al.* (2007) and Carberry and Sheridan (2007) by employing the reduced Froude number as the controlling parameter, where

$$Fr' = \frac{U}{\sqrt{(gD)(1-m^*)}} = \frac{\text{inertia force}}{\text{buoyancy force}} \quad (3)$$

Here, g is the acceleration due to gravity. High values of Fr' correspond to $\theta \rightarrow 90^\circ$, and have been found to correspond to peak amplitudes in the cylinder oscillation about its mean layover angle.

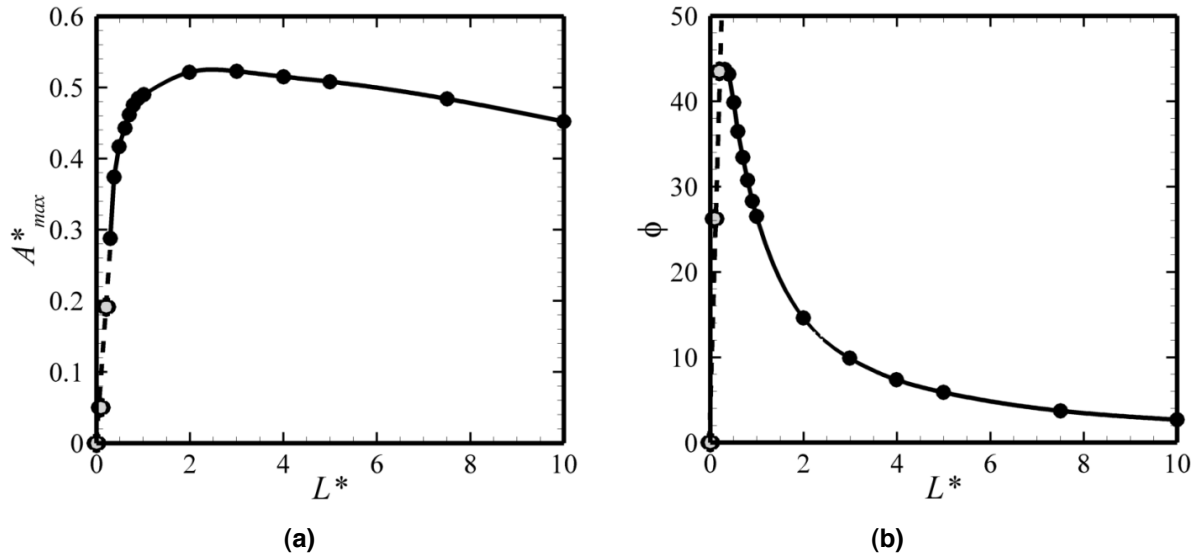


Figure 2. Amplitude of oscillation results as a function of L^* for $m^* = 0.2$ and $Fr' = 50$ – representing the highest amplitude response for all Fr' considered; (a) amplitude of oscillation defined as the peak translation of the cylinder away from its mean position; (b) angular amplitude of oscillation.

Figure 2 shows the peak amplitude of oscillation of the cylinder for $Fr' = 50$ for all tether lengths considered. Simulations at higher values of Fr' showed no deviation of peak amplitude, simulations at lower values of Fr' showed a reduction in peak amplitude. Figure 2(a) defines the amplitude as the peak displacement of the cylinder away from its mean position normalized by the

cylinder diameter. A peak in oscillation amplitude at $L^* = 2.0$ is observed in agreement with the findings of Ryan *et al.* (2007). The oscillations at this tether length are noteworthy with amplitudes greater than $0.5D$, quite significant considering the relatively low Reynolds number. Figure 2(b) again shows the variation of oscillation amplitude; however this time defined as the angular amplitude of oscillation about the pivot point. The two definitions are related through

$$A^* = L^* \sin(\phi). \quad (4)$$

Equation 4, coupled with the layout of the system (figure 1), allows us to deduce that $\phi \rightarrow 0$ as $L^* \rightarrow \infty$, and $A^*, \phi \rightarrow 0$ as $L^* \rightarrow 0$, in line with our observations in figure 2. However, within this range of L^* , we note two distinct trends in ϕ .

For $L^* < 0.3$, ϕ is observed to increase linearly with L^* . This may be understood by assuming that the fluid forces acting on the cylinder do not alter appreciably across the range $L^* = [0, 0.3]$. With this assumption, the amplitude of the moment acting to oscillate the body varies linearly with L^* . In addition, the moment of inertia of the system (equation 2) does not change appreciably across this range; indeed for tether lengths below $L^{*2} \approx 1/8$, the moment of inertia is virtually independent of any variation in tether length. Thus it is the linear increase in the amplitude of the moment acting on the body which results in the linear increase in oscillation amplitude. This assumes that the shedding frequency is far from the natural frequency of the system.

For $L^* \geq 0.3$ a decay in ϕ is noted, which in general is found to fit the general trend

$$\phi = \frac{a}{L^*}. \quad (5)$$

Here, the coefficient a is dependent on the cylinder mass ratio and flow Reynolds number. For our case, an excellent fit is observed when $a = 28.12$. The form of equation 5 may be derived through inspection of the equations of motion in a manner similar to that described by Govardhan and Williamson (2000). The peak in A^* observed by Ryan *et al.* (2007) is therefore due to the variation in ϕ , couple with the definition of A^* (equation 4).

Snapshots of the vortex structures in the wake of the tethered cylinder are shown in figure 3 for all tether lengths considered. In each case $Fr = 50$ corresponding to $\theta \approx 90^\circ$. This value was chosen such that the effect of varying L^* could be observed without the complications induced by a finite mean lift coefficient and the accompanying vortex pairing in the wake and mean angle at which the wake is shed.

For $L^* = 0.1$, the vortex structures are not dissimilar to the Karman vortex street observed from a stationary cylinder, which is anticipated given the very low A^* observed. As L^* is increased to 0.3 (figure 3b), a significantly different wake is observed. Here $A^* \approx 0.3$, and this has proved sufficient to alter the wake to form a double shear layer similar to that observed by Dusek *et al.* (1994) for a fixed cylinder. The double shear layer is observed to become unstable approximately fifteen diameters downstream and forms a Karman wake thereafter. This double shear layer wake is observed for the range $L^* = [0.3, 1.0]$, corresponding to cylinder oscillation amplitudes less than $0.5D$. The width of the double shear layer increases with increasing tether length.

As the tether length is increased to $L^* = 1.5$, the double shear layer wake is replaced with a 'P+S' structure described experimentally by Williamson and Roshko (1988) and observed by Blackburn and Henderson (1999) for the case of an oscillating cylinder at low Reynolds number. In agreement with the current findings, Blackburn and Henderson (1999) report a very small mean positive lift for this wake structure. For $L^* = 2.0$, the near-wake is similar to the Karman vortex street, however instabilities in the wake cause the formation of a double shear layer approximately seven diameters downstream of the cylinder prior to a further instability of the double shear layer

further downstream. For $L^* = 5.0$ and $L^* = 10.0$, the formation length is considerably longer and appears to increase with tether length.

The natural frequency of the system is dependent on the fluid forces acting on the cylinder, and cannot be predicted accurately *a priori*. Without this knowledge, a reduced velocity (U^*) or oscillation frequency ratio (f^*) cannot be defined, making comparison with the freely oscillating cylinder difficult. However, direct comparison of the wake structures found for the tethered cylinder with that of the freely oscillating cylinder (at the same Reynolds number) allows for a direct comparison of the mechanisms governing oscillation to be made. The strong similarity in the response of both systems makes this possible.

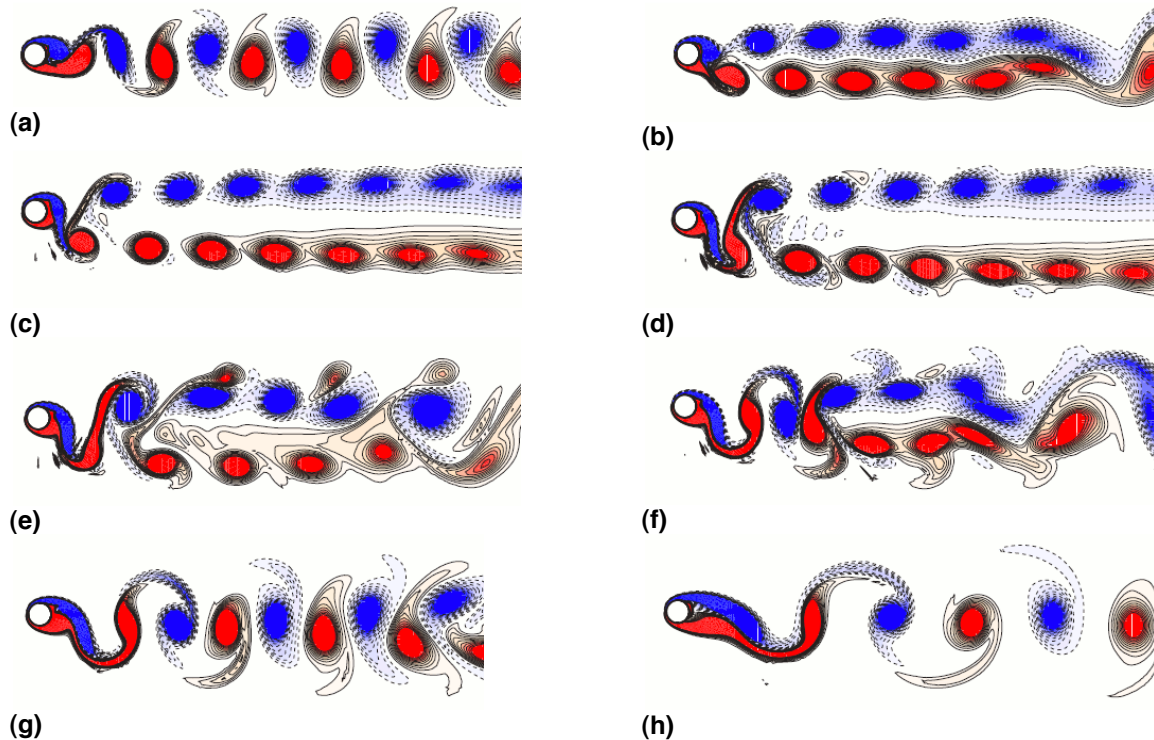


Figure 3. Instantaneous snapshots of the span-wise vorticity field, ω_z , as a function of tether length. Contours are evenly spaced over the range (blue) $-1 \leq \omega_z \leq 1$ (red). All images are at the instant when the cylinder reaches the top of the oscillating cycle; (a) $L^* = 0.1$; (b) $L^* = 0.3$; (c) $L^* = 0.5$; (d) $L^* = 1.0$; (e) $L^* = 1.5$; (f) $L^* = 2.0$; (g) $L^* = 5.0$; (h) $L^* = 10.0$.

References

- Blackburn, H.M. & Henderson, R. D. (1999) A study of two-dimensional flow past an oscillating cylinder. *Journal of Fluid Mechanics* **385**, 255-286.
- Carberry, J. & Sheridan, J. (2007) Wake states of a tethered cylinder. *Journal of Fluid Mechanics* **592**, 1-21.
- Dusek, J., Fraunie, P. & Le Gal, P. (1994) Local analysis of the onset of instability in shear flows. *Physics of Fluids*, **6**, 172-186.
- Khalak, A. & Williamson, C.H.K. (1999) Motions, forces and mode transitions in vortex-induced vibrations at low mass-damping. *Journal of Fluids and Structures*, **13**, 813-851.
- Govardhan, R. N. & Williamson, C.H.K. (2000) Modes of vortex formation and frequency response of a freely vibrating cylinder. *Journal of Fluid Mechanics*, **420**, 85-130.
- Govardhan, R. N. & Williamson, C.H.K. (2003) Resonance forever: existence of a critical mass and an infinite regime of resonance in vortex-induced vibration. *Journal of Fluid Mechanics*, **473**, 147-166.
- Ryan, K., Thompson, M.C. & Hourigan, K. (2007) The effect of mass ratio and tether length on the flow around a tethered cylinder. *Journal of Fluid Mechanics* **591**, 117-144.
- Williamson, C. H. K. & Roshko, A. (1988) Vortex formation in the wake of an oscillating cylinder. *Journal of Fluids and Structures*, **2**, 355-381.